Electronic Supplementary information

Experimental

Materials: Sodium gluconate ($C_6H_{11}NaO_7$, 99.0%), sodium carbonate (Na_2CO_3, 99.0%), hydrochloric acid (HCl, 99.0%), and ethanol (C_2H_6O, 99.0%), ammonium chloride (NH_4Cl), salicylic acid ($C_7H_6O_3$), sodium citrate dehydrate ($C_6H_5Na_3O_7·2H_2O$), *p*-dimethylaminobenzaldehyde ($C_9H_{11}NO$), sodium nitroferricyanide dihydrate ($C_5FeN_6Na_2O·2H_2O$), benzyl disulfide (BDS), sodium hypochlorite solution (NaClO) and graphene oxide (GO) powder were purchased from Aladdin Ltd. (Shanghai, China). Nafion (5 wt%) solution was purchased from Sigma-Aldrich Chemical Reagent Co., Ltd. Hydrochloric acid, nitric acid, sulfuric acid, hydrogen peroxide, hydrazine monohydrate ($N_2H_4·H_2O$) and ethyl alcohol (C_2H_5OH) were purchased from Beijing Chemical Corp. (China). chemical Ltd. in Chengdu. The ultrapure water used throughout all experiments was purified through a Millipore system. All reagents were analytical reagent grade without further purification.

Preparation of S-G and G: S-graphene was synthesized by directly annealing GO and BDS in argon. The anneal treatment was carried out in a tube furnace with high purity argon as protective ambient. The detailed procedure is as follows. GO and BDS with mass ratio of GO and BDS of 1:2 was ultrasonically dispersed in ethanol for about 30 min. The resulting suspension was spread onto an evaporating dish and dried, forming a uniform solid mixture. The mixture was placed into a quartz tube with argon atmosphere and annealed at 1050 °C. After that, the sample was cooled to room temperature under ambient Ar and collected from the quartz tube. For comparison, undoped G was prepared GO without BDS was treated under the same condition.

Characterizations: Transmission electron microscopy (TEM) images were collected on a HITACHI H-8100 electron microscopy (Hitachi, Tokyo, Japan) operated at 200 kV. XPS measurements were performed on an ESCALABMK II X-ray photoelectron spectrometer using Mg as the exciting source. Raman spectra were obtained by a Renishaw inVia confocal

Raman microprobe under 532 nm laser excitation. The absorbance data of spectrophotometer were acquired on SHIMADZU UV-1800 UV-Vis spectrophotometer.

Electrochemical Measurements: Electrochemical NRR measurements were performed in a two-compartment cell separated by Nafion membrane using a CHI660E electrochemical analyzer (CH Instruments, Inc.). The electrochemical experiments were carried out with a three-electrode configuration using graphite plate as the counter electrode and Ag/AgCl/saturated KCl as the reference electrode. The working electrode was a modified. In a typical synthesis of electrode, 10 mg of the catalyst was dispersed in 1 mL of water containing Nafion solution (5 wt%), followed by ultrasonic treatment for 30 min to form a homogeneous ink. Then, 10 μL of the ink was loaded onto a carbon paper electrode with area of 1 x 1 cm^2 and dried under ambient condition, the catalyst loading mass is 0.1 mg. The potentials reported in this work were converted to reversible hydrogen electrode (RHE) scale via calibration with the following equation: E (vs. RHE) = E (vs. Ag/AgCl) + 0.256 V and the presented current density was normalized to the geometric surface area. For electrochemical N_2 reduction, chrono-amperometry tests were conducted in N_2-saturated 0.1 M HCl solution (the HCl electrolyte was purged with N_2 for 30 min before the measurement).

Determination of NH_3: Concentration of produced NH_3 was spectrophotometrically determined by the indophenol blue method.[1] Typically, 2 mL electrolyte was taken from the cathodic chamber, and then 2 mL of 1 M NaOH solution containing 5% salicylic acid and 5% sodium citrate was added into this solution. Subsequently, 1 mL of 0.05 M NaClO and 0.2 mL of 1% $C_5FeN_6Na_2O \cdot 2H_2O$ were add into the above solution. After standing at room temperature for 2 h, the UV-Vis absorption spectrum was measured at a wavelength of 655 nm. The concentration-absorbance curves were calibrated using standard NH_3 solution with a serious of concentrations. The fitting curve (y = 0.3713x + 0.0515, R^2 = 0.999) shows good linear relation of absorbance value with NH_3 concentration by three times independent calibrations.

Determination of N$_2$H$_4$: The N$_2$H$_4$ presented in the electrolyte was estimated by the method of Watt and Chrisp.[2] A mixed solution of 5.99 g C$_9$H$_{11}$NO, 30 mL HCl and 300 ml ethanol was used as a color reagent. Calibration curve was plotted as follow: firstly, preparing a series of reference solutions; secondly, adding 5 mL above prepared color reagent and stirring 20 min at room temperature; finally, the absorbance of the resulting solution was measured at 455 nm, and the yields of N$_2$H$_4$ were estimated from a standard curve using 5 mL residual electrolyte and 5 mL color reagent. Absolute calibration of this method was achieved using N$_2$H$_4$·H$_2$O solutions of known concentration as standards, and the fitting curve shows good linear relation of absorbance with N$_2$H$_4$·H$_2$O concentration (y = 1.0734 x + 0.0318, R^2 = 0.999) by three times independent calibrations.

Calculations of NH$_3$ formation rate and FE: The FE for N$_2$ reduction was defined as the amount of electric charge used for synthesizing NH$_3$ divided the total charge passed through the electrodes during the electrolysis. The total amount of NH$_3$ produced was measured using colorimetric methods. Assuming three electrons were needed to produce one NH$_3$ molecule, the FE could be calculated as follows:

Ammonia formation was calculated using the following equation:

Ammonia formation rate = [NH$_4^+$]×V/(m×t)

FE was calculated according to following equation:

FE = 3×F×[NH$_4^+$]×V/(17×Q)

Where [NH$_4^+$] is the measured NH$_4^+$ ion concentration; V is the volume of the cathodic reaction electrolyte; t is the potential applied time; m is the loaded quality of catalyst; F is the Faraday constant; and Q is the quantity of applied electricity.

Computational method: All electron spin-polarized DFT methods implemented in the DMol3 module of Material Studio package have been employed for all present calculations.[3,4] The generalized gradient approximation Perdew-Burke-Ernzerhof (PBE) exchange-correlation functional is adopted.[5] The van der Waals interaction is described using the empirical

correction scheme of Grimme.[6] To expand the electronic wavefunction, the double numerical plus polarization (DNP) basis set is used.[7] Self-consistent field (SCF) calculations are performed with a total energy convergence criterion of 10^{-6} hartree. Since bulk water layer slightly stabilizes NRR intermediates,[8] we have therefore adopted the conductor-like screening model (COSMO) to implicitly consider solvent effects.[9]

Twelve sulfur-doped models have been constructed in our work. Eight of them are sulfur-doped graphene models. For them, a 6×6 two-dimensional graphene supercell has been used. In DFT calculations, a 5×5×1 Monkhorst–Pack k-points are used. However, for the S-doped graphene nanorribon models, both 4×5 zigzag and 9×3 armchair graphene nanoribbons are employed in which a 1×1×5 Monkhorst–Pack k-points are used in the DFT calculations. In both situations, to avoid artificial interaction a more than 15 Å vacuum layer is used between two neighboring slabs. Fig. S9 schematically illustrates our constructed sulfur-doped graphene models.

Six net proton coupled electron transfer (PCET) steps are involved in NRR processes ($N_2 + 6H^+ + 6e^- \rightarrow NH_3$). According to previous theoretical studies,[10] gaseous H_2 is employed as the proton source due to its convenience of simulating the anode reaction i.e. $H_2 \leftrightarrow 2(H^+ + e^-)$. Every PCET step involves the transfer of a proton coupled with an electron from solution to an adsorbed species on the surface of electrocatalyst. The Gibbs free energy change (ΔG) of every elemental step is calculated by using the standard hydrogen electrode (SHE) model proposed by Nørskov et al.,[11-13] which uses a half of chemical potential of hydrogen molecule as the chemical potential of a proton-electron pair. In detail, the free energy change is defined: $\Delta G = \Delta E + \Delta ZPE - T\Delta S + \Delta G_{pH} + \Delta G_U$, where ΔE is the reaction energy directly obtained from DFT calculations; ΔZPE is the change in zero-point energy; The is temperature (298.15 K); and ΔS is the change in entropy. $\Delta G_U = -neU$, where n is the number of electrons transferred and U is the electrode potential. ΔG_{pH} is the correction of the H^+ free energy by the concentration, determined as $\Delta G_{pH} = 2.303 \times k_B T \times pH$ (or $0.059 \times pH$), where k_B is the

Boltzmann constant and the value of pH is assumed to be zero. The zero-point energies and entropies of the NRR species are determined from the vibrational frequencies in which only the adsorbed species' vibrational modes are computed explicitly and the electrocatalyst sheet is fixed. The entropies and vibrational frequencies of gas phase molecules are taken from the NIST database [http://cccbdb.nist.gov/].

We have calculated the adsorption energy of the N_2 and NNH species on the catalyst sheet. The adsorption energy of X species $E_{ads}(X)$ is calculated as the energy difference

$E_{ads}(X) = -[E(\text{total}) - E(\text{surface}) - E(X)]$

where $E(\text{surface})$, $E(X)$, and $E(\text{total})$ are the potential energies of the clean surface, gas-phase X species, and the adsorbed X spacies, respectively.
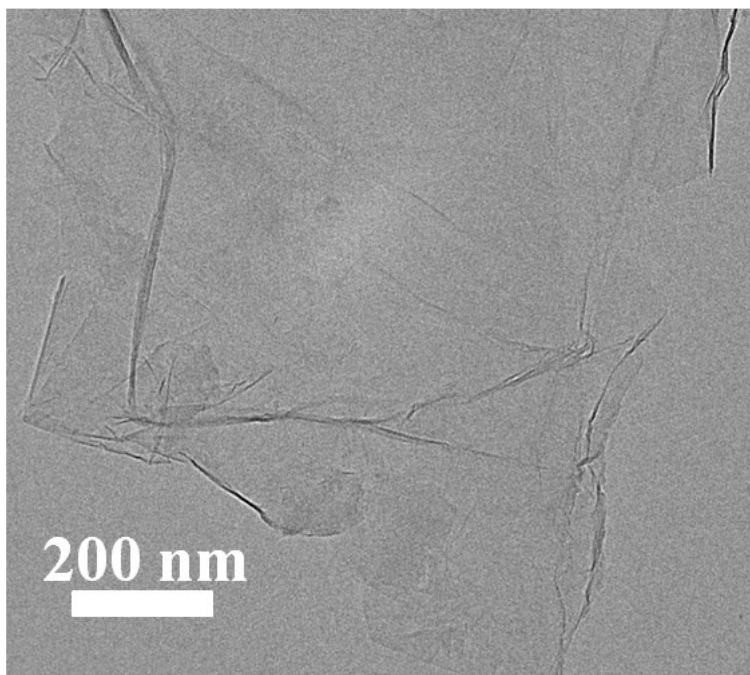
Fig. S1. TEM image of G.
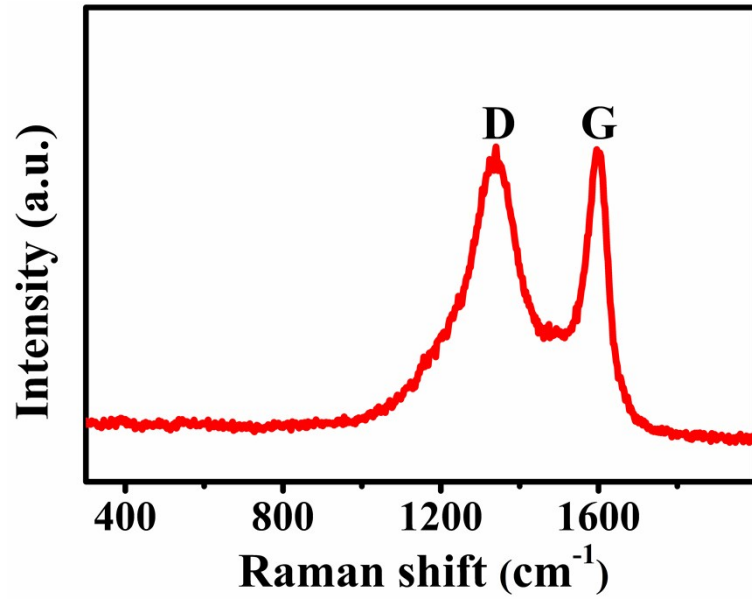
Fig. S2. Raman spectrum of S-G.
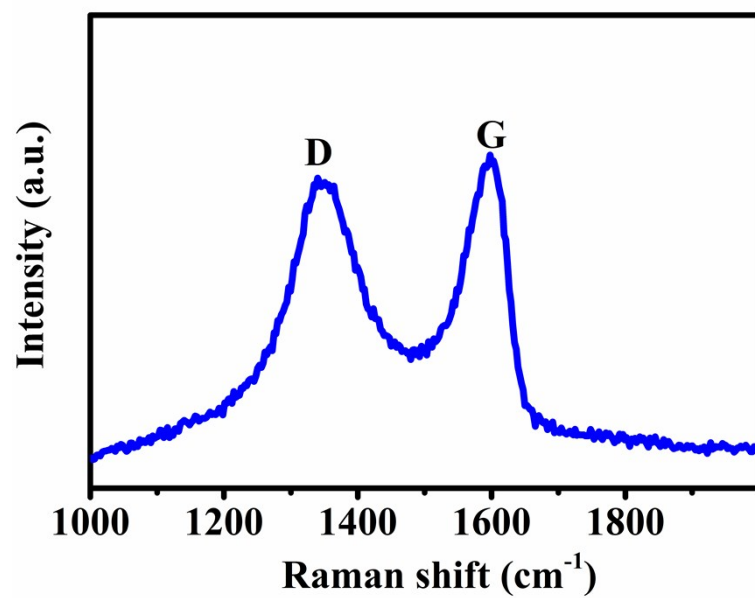
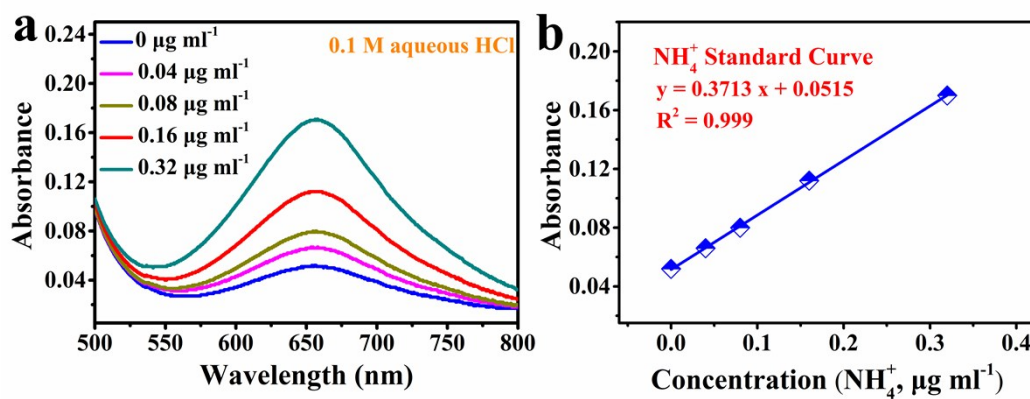**Fig. S3.** Raman spectrum of G.

Fig. S4. (a) UV-Vis absorption spectra of indophenol assays with NH_4^+ ions after incubated for 2 h at room temperature. (b) Calibration curve used for estimation of NH_4^+.
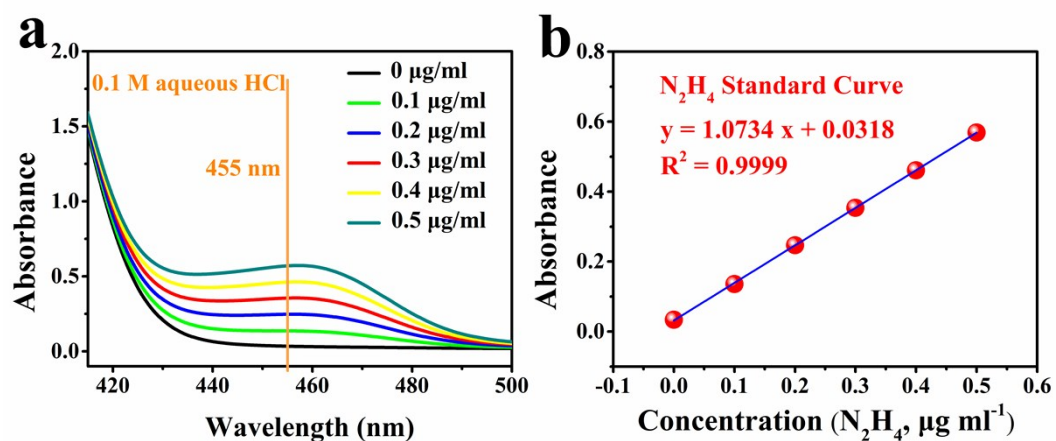
Fig. S5. (a) UV-Vis absorption spectra of various N_2H_4 concentrations after adding into chemical indicator by the method of Watt. (b) Calibration curve used for calculation of N_2H_4 concentrations.
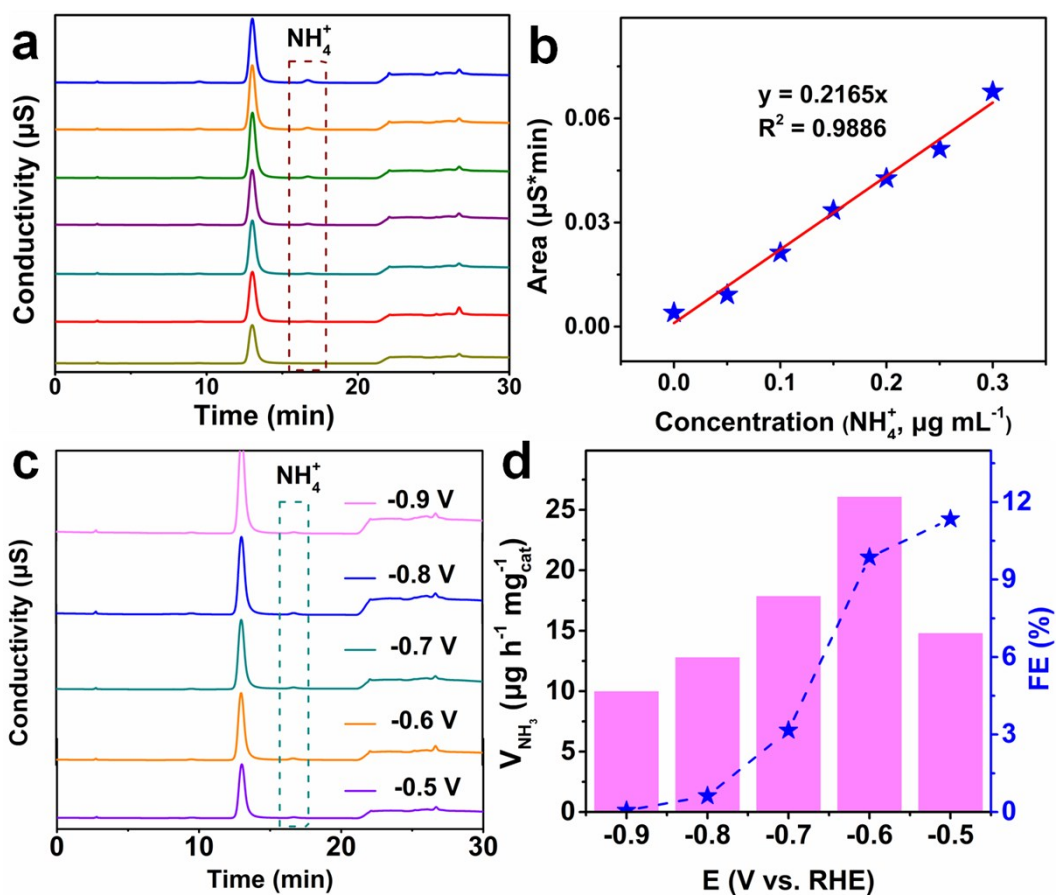
Fig. S6. (a) Ion chromatogram analysis for the NH_4^+ ions. (b) Calibration curve used for estimation of NH_4^+. (c) Ion chromatogram for the electrolytes at a series of potentials after electrolysis for 2 h. (d) V_{NH_3} and FEs for S-G/CP at corresponding potentials.
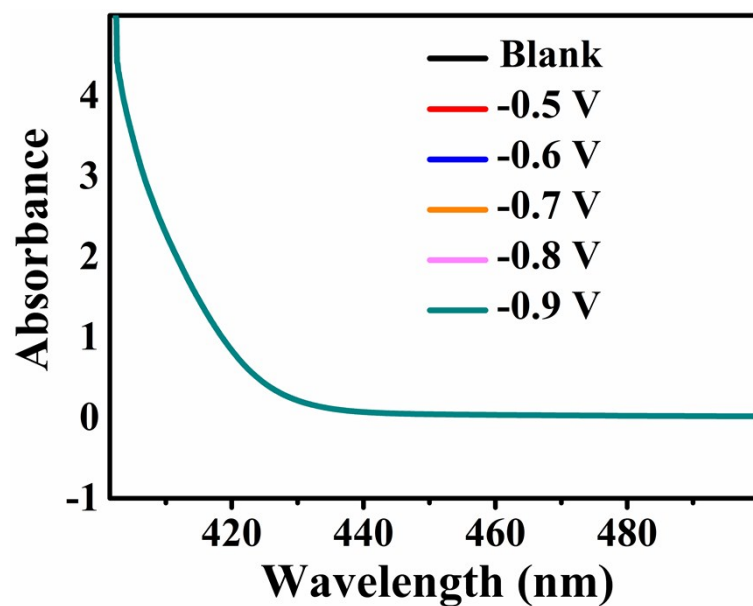
Fig. S7. UV-Vis absorption spectra of the electrolytes estimated by the method of Watt and Chrisp before and after 2 h electrolysis in N_2 atmosphere at each given potential at ambient conditions using S-G/CP as the working electrode.
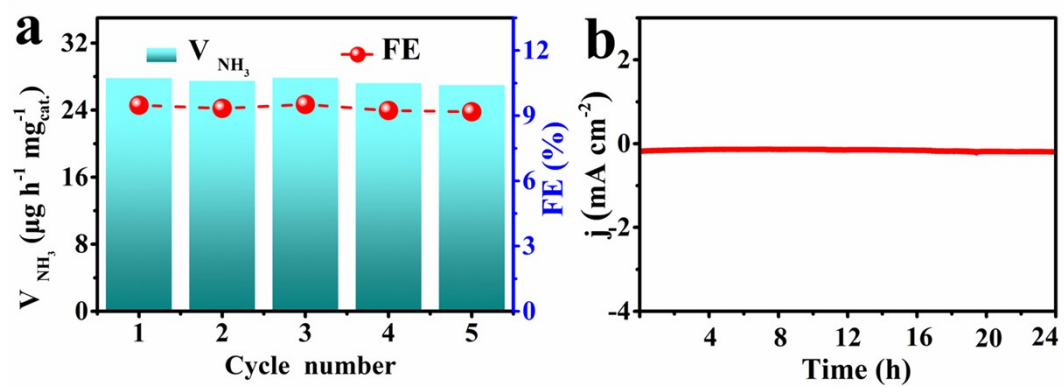
Fig. S8. (a) Recycling tests at potential of –0.6 V for S-G. (b) Time-dependent current density curve for S-G catalyst at the potential of –0.6 V for 24 h.
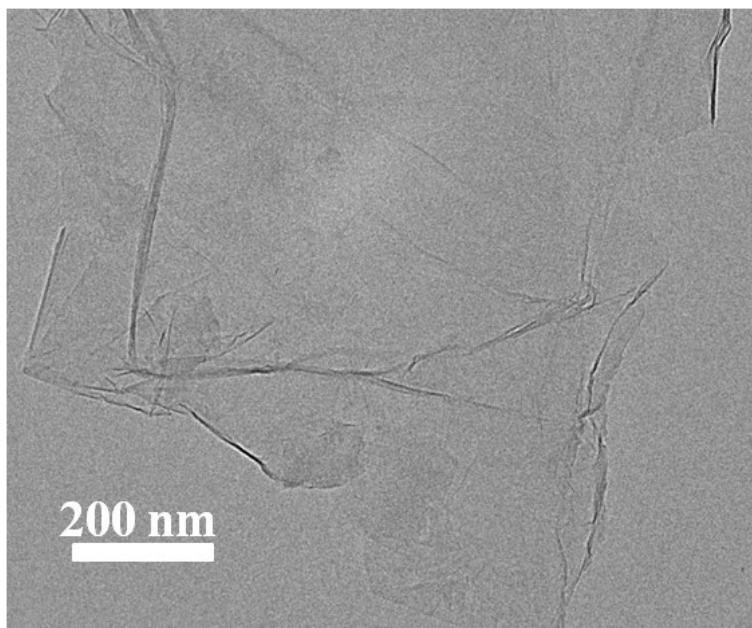
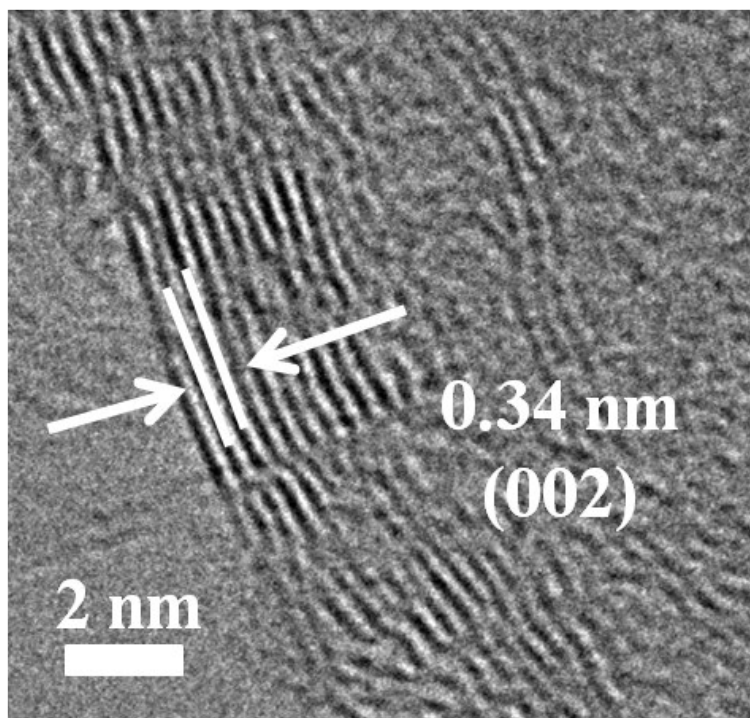**Fig. S9.** TEM image for S-G after stability test.
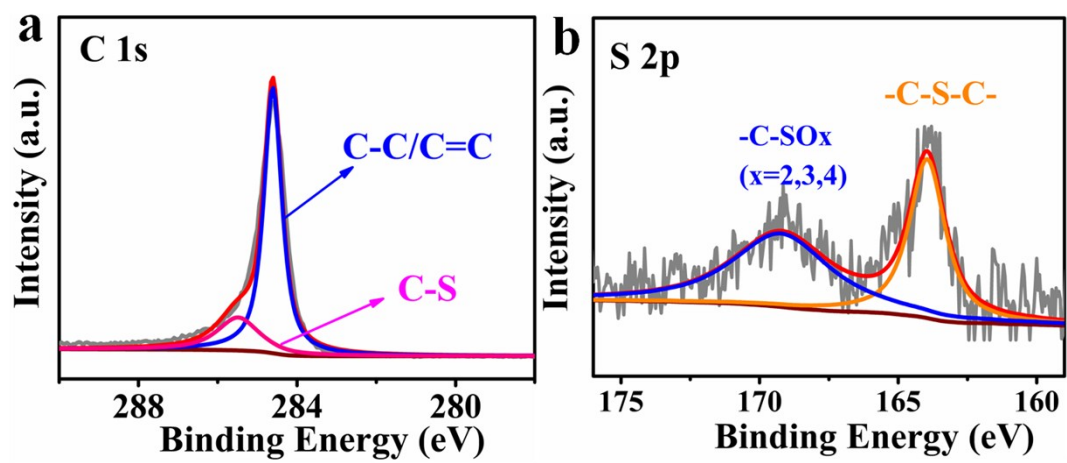
Fig. S10. HRTEM image for S-G after stability test.

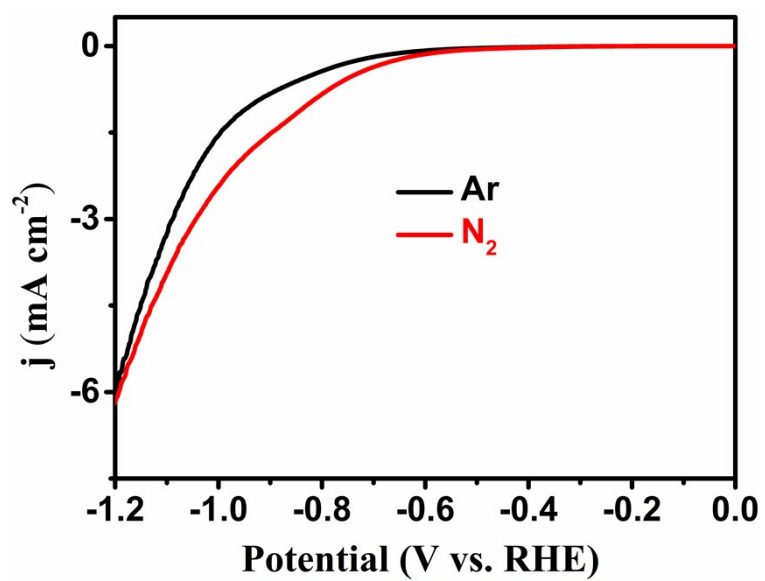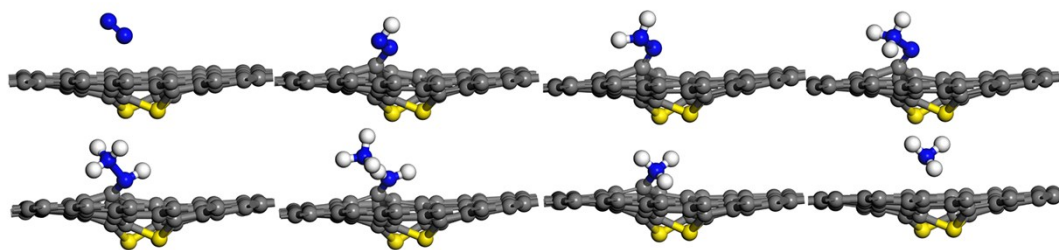**Fig. S11.** XPS spectra of S-G in the (a) C 1s and (b) S 2p regions after stability test.

Fig. S12. LSV curves of S-G/CP in Ar- and N_2-saturated 0.1 M HCl with a scan rate of 5 mV s^{-1} after stability test.

Distal   Pathway

Alternating Pathway

Fig. S13. DFT optimized geometric structures of the NRR intermediates of model 1. Color code: carbon in gray, sulfur in yellow, hydrogen in white.

Distal Pathway

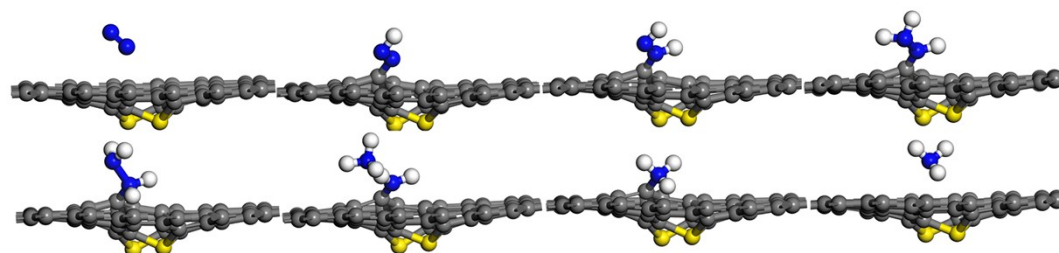
Alternating Pathway

Fig. S14. DFT optimized geometric structures of the NRR intermediates of model 2. Color code: carbon in gray, sulfur in yellow, hydrogen in white.

Fig. S15. DFT calculated energy profile for the electrocatalytic N_2 reduction reaction on sulfur-doped graphene based on models 1 (a) and 2 (b) under the electrode potentials of -0.6 V.
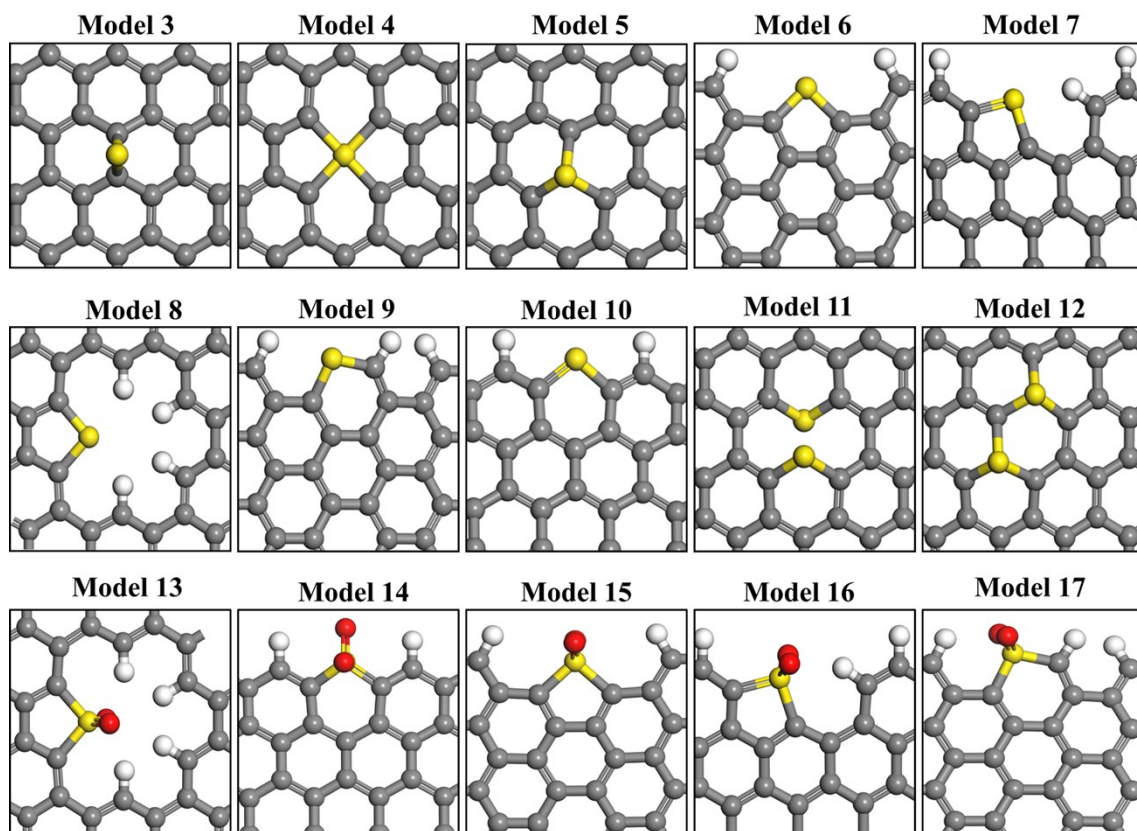
Fig. S16. Our constructed sulfur-doped graphene models 3-17 for the exploration of the NRR active sites and mechanisms (color code: carbon in gray, sulfur in yellow, hydrogen in white, and oxygen in red). The models 1 and 2 are discussed in the main text.

Distal Pathway
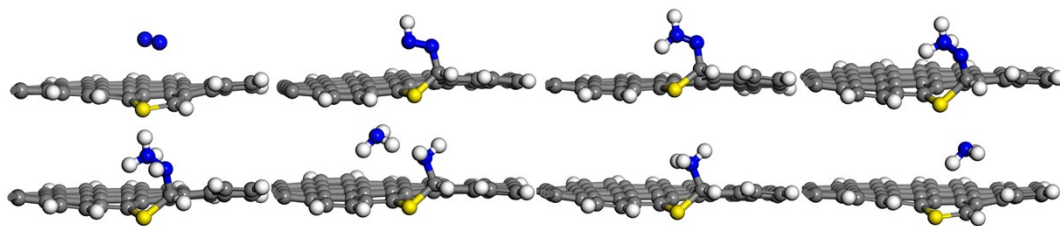
Alternating Pathway

Fig. S17. DFT optimized geometric structures of the NRR intermediates of model 9. Color code: carbon in gray, sulfur in yellow, hydrogen in white.
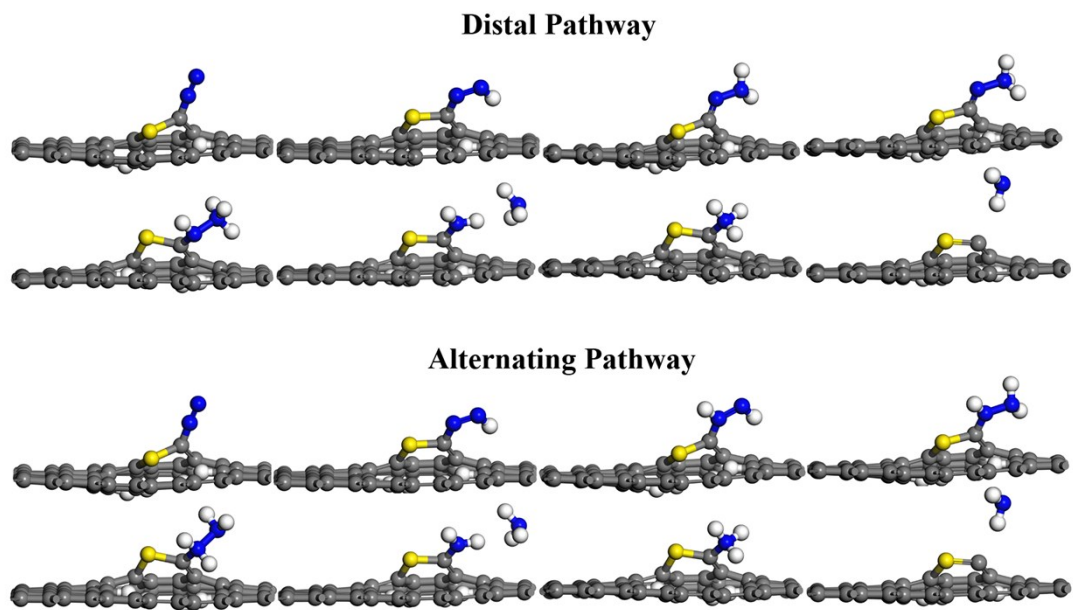
Fig. S18. DFT optimized geometric structures of the NRR intermediates of model 12. Color code: carbon in gray, sulfur in yellow, hydrogen in white.
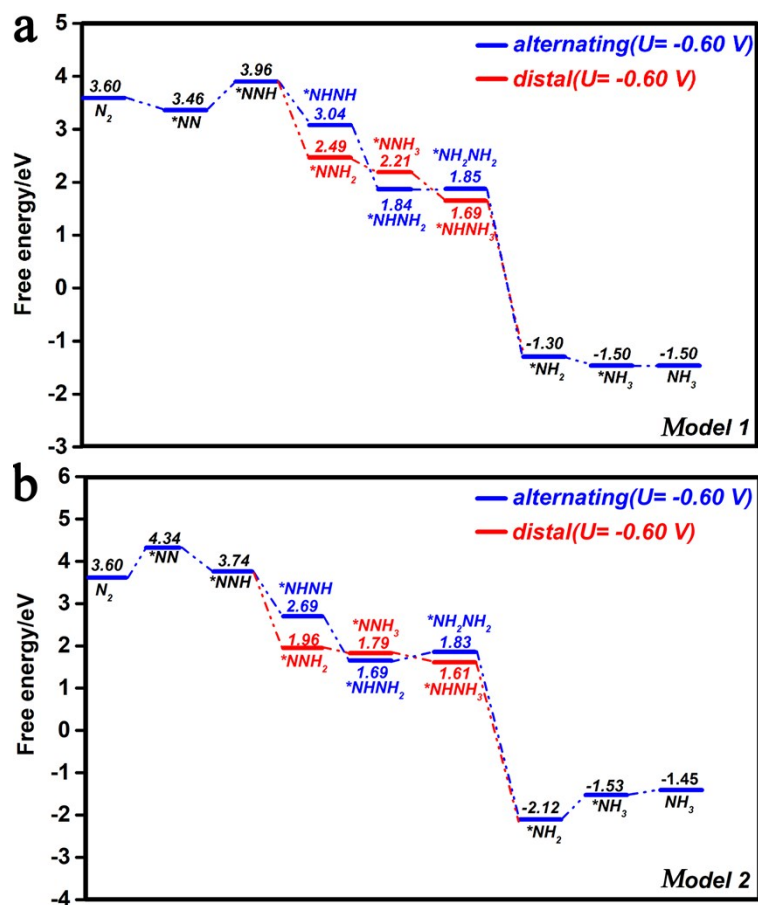
Distal Pathway

Alternating Pathway

Fig. S19. DFT optimized geometric structures of the NRR intermediates of model 17. Color code: carbon in gray, sulfur in yellow, hydrogen in white, oxygen in red.
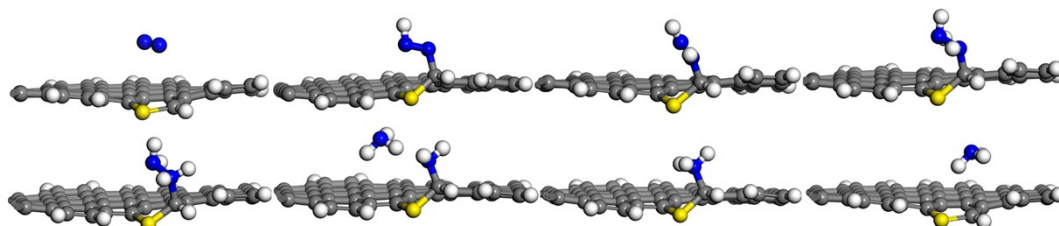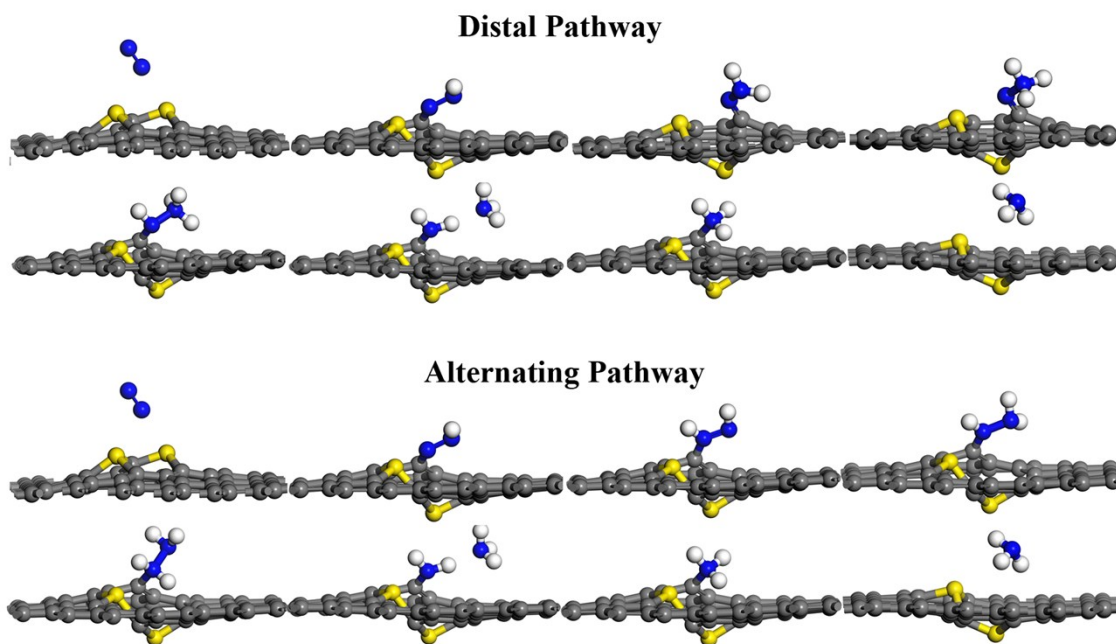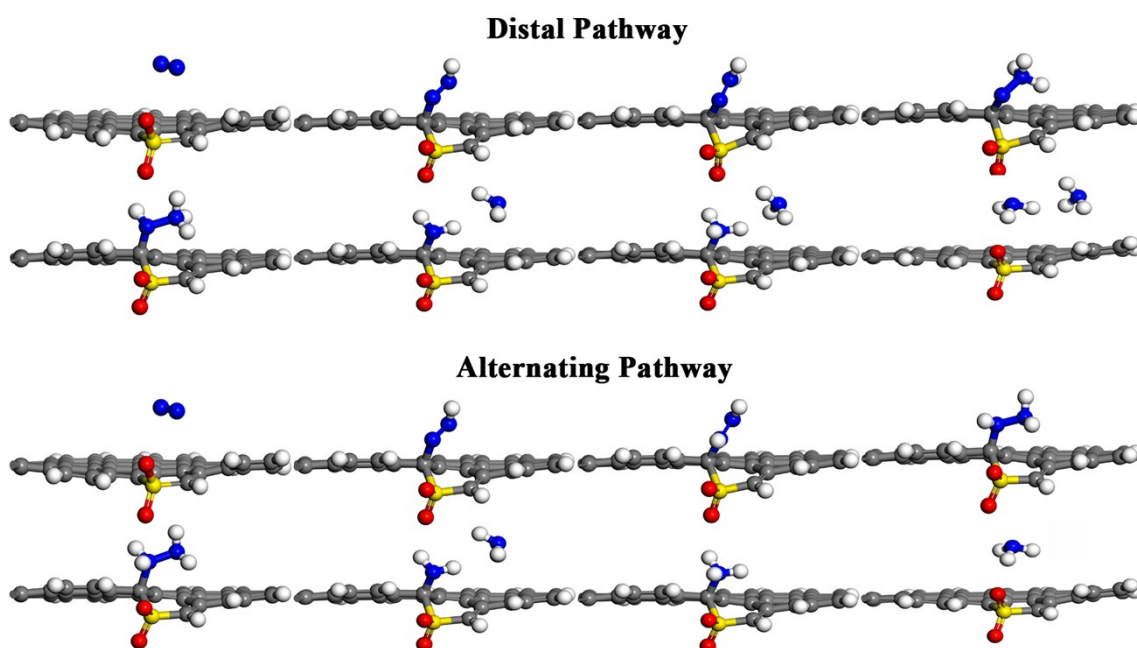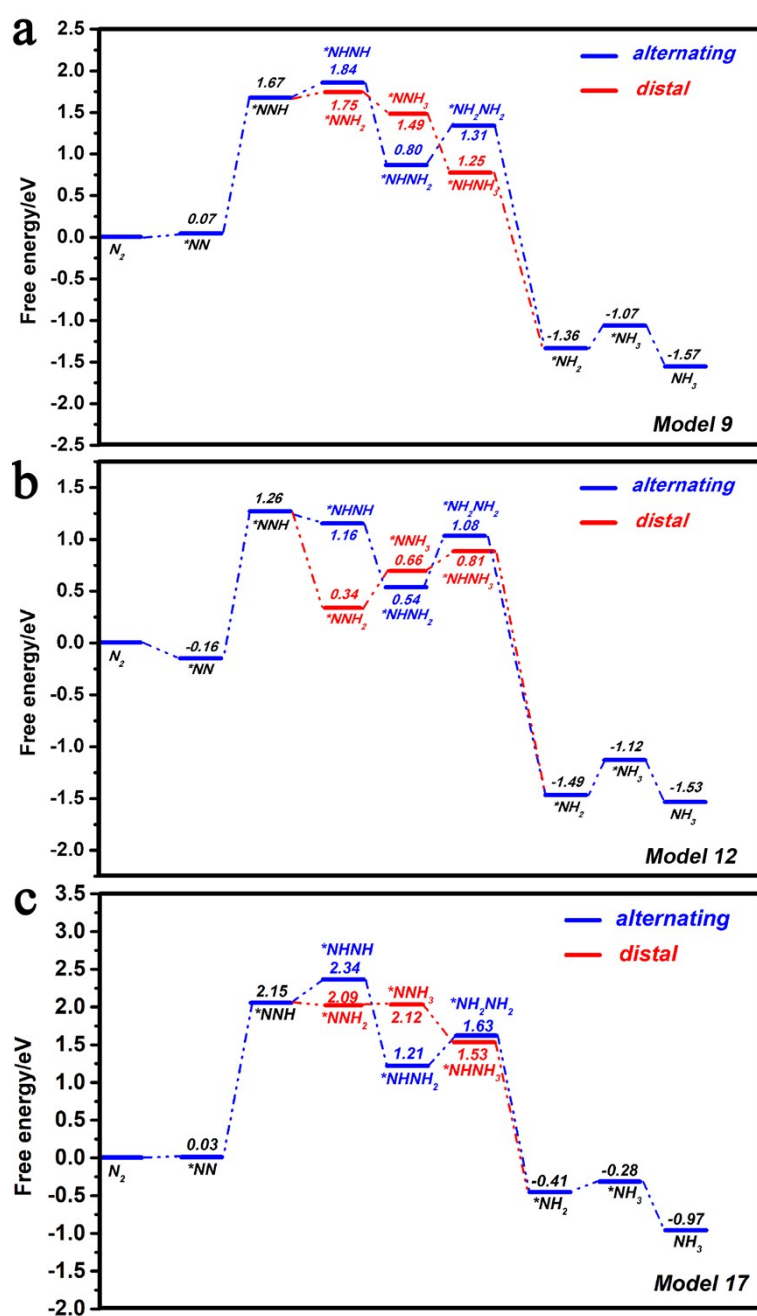
Fig. S20. DFT calculated free energy profiles (eV) of the alternative (blue) and distal (red) NRR pathways of models 9, 12, and 17 in Figure S14. Those for models 1 and 2 are in the main text.

Table S1. Comparison of electrocatalytic N_2 reduction performance for S-G with other aqueous-based electrocatalysts in acids at ambient conditions.

Catalyst	Electrolyte	NH$_3$ yield	FE%	Ref.
S-G/CP	0.1 M HCl	27.3 μg h^{-1} mg^{-1}$_{cat.}$	11.5	This work
α-Au/CeO$_x$-RGO	0.1 M HCl	8.31 μg h^{-1} mg^{-1}$_{cat.}$	10.1	14
TA-reduced Au/TiO$_2$	0.1 M HCl	21.4 μg h^{-1} mg^{-1}$_{cat.}$	8.11	15
Bi$_4$V$_2$O$_{11}$/CeO$_2$	0.1 M HCl	23.21 μg h^{-1} mg^{-1}$_{cat.}$	10.16	16
Mo nanofilm	0.01 M H$_2$SO$_4$	1.89 μg h^{-1} cm^{-2}	0.72	17
N-doped porous carbon	0.05 M H$_2$SO$_4$	23.8 μg h^{-1} mg^{-1}$_{cat.}$	1.42	18
N-doped porous carbon	0.1 M HCl	15.7 μg h^{-1} mg^{-1}$_{cat.}$	1.45	19
Boron-doped graphene	0.05 M H$_2$SO$_4$	9.8 μg h^{-1} cm^{-2}	10.8	20
Polymeric carbon nitride	0.1 M HCl	8.09 μg h^{-1} mg^{-1}$_{cat.}$	11.59	21
MoO$_3$	0.1 M HCl	29.43 μg h^{-1} mg^{-1}cat.	1.9	22
Mo$_2$N nanorod	0.1 M HCl	78.4 μg h^{-1} mg$_{cat.}$$^{-1}$	4.5	23
Nb$_2$O$_5$ nanofiber	0.1 M HCl	43.6 μg h^{-1} mg^{-1}$_{cat.}$	9.26	24
B$_4$C	0.1 M HCl	26.57 μg h^{-1} mg^{-1}$_{cat.}$	15.95	25
Ti$_3$C$_2$T$_x$ nanosheet	0.1 M HCl	20.4 μg h^{-1} mg^{-1}$_{cat.}$	9.3	26
Mo$_2$C nanorod	0.1 M HCl	95.1 μg h^{-1} mg^{-1}$_{cat.}$	8.13	27
d-TiO$_2$/TM	0.1 M HCl	1.24×10^{-10} mol s^{-1} cm^{-2}	9.17	28
VN	0.1 M HCl	2.48×10^{-10} mol^{-1} s^{-1} cm^{-2}	3.58	29
Cr$_2$O$_3$-rGO	0.1 M HCl	33.3 μg h^{-1} mg^{-1}$_{cat.}$	7.33	30

Table S2. Adsorption energies (eV) of N_2 and NNH species on models 1-17, in which '-' represents that the species cannot be stably adsorbed on the surfaces.

	1	2	3	4	5	6	7	8	9
N_2	0.22	-0.37	0.15	0.23	0.14	0.04	0.14	0.10	0.12
NNH	1.65	1.73	-	0.10	0.14	-0.09	-0.07	-	0.99
	10	11	12	13	14	15	16	17	
N_2	0.04	0.14	0.21	0.16	0.12	0.11	0.12	0.11	
NNH	-0.04	0.15	1.37	0.21	-0.32	-	-0.03	0.43	

Reference

1   D. Zhu, L. Zhang, R. E. Ruther and R. J. Hamers, *Nat. Mater.,* 2013, **12**, 836–841.

2   G. W. Watt and J. D. Chrisp, *Anal. Chem.,* 1952, **24**, 2006–2008.

3   B. Delley, *J. Chem. Phys.,* 1990, **92**, 508–517.

4   B. Delley, *J. Chem. Phys.*, 2000, **113**, 7756–7764.

5   J. P. Perdew, K. Burke and M. Ernzerhof, *Phys. Rev. Lett.*, 1996, **77**, 3865.

6   S. Grimme, *J. Comput. Chem.*, 2006, **27**, 1787–1799.

7   P. Liu and J. A. Rodriguez, *J. Am. Chem. Soc.*, 2005, **127**, 14871–14878.

8   E. Skúlason. T. Bligaard, S. Gudmundsdóttir, F. Studt, J. Rossmeisl, F. A. Pedersen, T. Vegge, H. Jónsson and J. K. Nørskov, *Phys. Chem. Chem. Phys.,* 2012, **14**, 1235–1245.

9   A. Klamt and G. Schüürmann, *J. Chem*. Soc., Perkin Trans. 2, 1993, **0**, 799–805.

10 K. C. MacLeod, S. F. McWilliams, B. Q. Mercado and P. L. Holland, *Chem. Sci.,* 2016, **7**, 5736–5746.

11 J. K. Nørskov, J. Rossmeisl, A. Logadottir and L. Lindqvist, *J. Phys. Chem. B,* 2004, **108**, 17886–17892.

12 J. Rossmeisl, A. Logadottir and J. K. Nørskov, *Chem. Phys.,* 2005, **319**, 178–184.

13 A. A. Peterson, F. Abild-Pedersen, F. Studt, J. Rossmeisl and J. K Nørskov, *Energy Environ. Sci.,* 2010, **3**, 1311–1315.

14 S. Li, D. Bao, M. Shi, B. Wulan, J. Yan and Q. Jiang, *Adv. Mater.,* 2017, **29**, 1700001.

15 M. Shi, D. Bao, B. R. Wulan, Y. Li, Y. Zhang, J. Yan and Q. Jiang, *Adv. Mater,* 2017, **29**, 1606550.

16 C. Lv, C. Yan, G. Chen, Y. Ding, J. Sun, Y. Zhou and G. Yu, *Angew. Chem., Int. Ed.,* 2018, **57**, 6073–6076.

17 D. Yang, T. Chen and Z. Wang, *J. Mater. Chem. A*, 2017, **5**, 18967–18971.

18 Y. Liu, Y. Su, X. Quan, X. Fan, S. Chen, H. Yu, H. Zhao, Y. Zhang and J. Zhao, *ACS Catal.*, 2018, **8**, 1186−1191.

19 X. Yang, K. Li, D. Cheng, W. Pang, J. Lv, X. Chen, H. Zang, X. Wu, H. Tan, Y. Wang and Y. Li, *J. Mater. Chem. A,* 2018, **6**, 7762−7769.

20 X. Yu, P. Han, Z. Wei, L. Huang, Z. Gu, S. Peng, J. Ma and G. Zheng, *Joule,* 2018**, 2**, 1610–1622.

21 C. Lv, Y. Qian, C. Yan, Y. Ding, Y. Liu, G. Chen and G. Yu, *Angew. Chem., Int. Ed.,* 2018, **57**, 10246–10250.

22 J. Han, X. Ji, X. Ren, G. Cui, L. Li, F. Xie, H. Wang, B. Li and X. Sun, *J. Mater. Chem. A,* 2018, **6**, 12974–12977.

23 X. Ren, G. Cui, L. Chen, F. Xie, Q. Wei, Z. Tian and X. Sun, *Chem. Commun.,* 2018, **54**, 8474–8477.

24 J. Han, Z. Liu, Yo. Ma, G. Cui, F. Xie, F. Wang, Y. Wu, S. Gao, Y. Xu and X. Sun, *Nano Energy,* 2018, **52**, 264–270.

25 W. Qiu, X. Xie, J. Qiu, W. Fang, R. Liang, X. Ren, X. Ji, G. Cui, A. M. Asiri, G. Cui, B. Tang and X. Sun, *Nat. Commun.,* 2018, **9**, 3485.

26 J. Zhao, L. Zhang, X. Xie, X. Li, Y. Ma, Q. Liu, W. Fang, X. Shi, G. Cui and X. Sun, *J. Mater. Chem. A,* 2018, **6**, 24031–24035.

27 X. Ren, J. Zhao, Q. Wei, Y. Ma, H. Guo, Q. Liu, Y. Wang, G. Cui, A. M. Asiri, B. Li, B. Tang and X. Sun, *ACS Central Sci.,* 2019, **5**, 116–121.

28 L. Yang, T. Wu, R. Zhang, H. Zhou, L. Xia, X. Shi, H. Zheng, Y. Zhang and X. Sun, *Nanoscale,* 2019*,* **11***,* 1555–1562.

29 X. Zhang, R. Kong, H. Du, L. Xia and F. Qu, *Chem. Commun.*, 2018, **54**, 5323–5325.

30 L. Xia, B. Li, Y. Zhang, R. Zhang, L. Ji, H. Chen, G. Cui, H. Zheng, X. Sun, F. Xie and Q. Liu, *Inorg. Chem,.* 2019, **58**, 2257–2260.